The Pressure Anemometer—an Instrument for Adverse Circumstances

W. A. OOST

Royal Netherlands Meteorological Institute (KNMI), Wilhelminalaan 10, 3730 AE De Bilt, Netherlands

(Manuscript received 19 January 1983, in final form 5 July 1983)

ABSTRACT

A new instrument is presented to measure the wind vector under fouling circumstances, such as spray conditions just above the sea. It is in principle a combination of six pressure tubes, arranged in three mutually orthogonal sets of two. The tubes in each set point in opposite directions and are connected to the ports of a differential pressure transducer. From the readings of the three pressure transducers both the wind speed and direction can be derived. In order to keep the tubes clean, a continuous airflow is forced through them. In its present configuration, the pressure anemometer has a lower speed limit of 4 m s^{-1} and a frequency range of 0–35 Hz.

The instrument was compared with a sonic anemometer at a research platform off the Dutch coast. The results of this intercomparison show satisfactory agreement between the instruments. The new instrument, however, has a better high-frequency response.

1. Introduction

The crucial region in all theories and models for the description of small-scale air–sea interaction (e.g., Miles, 1957, 1959; Riley *et al.*, 1982; Janssen, 1982; Gent and Taylor, 1976; Gent, 1977; Chalikov, 1978; Melville 1977) is the one just above the water. This makes measurements in this region highly desirable, especially at high wind speeds, when the momentum transport is most intense. It is, however, a rather difficult region for measurements. Commercially available wind sensors are either too fragile (hot wires), too susceptible to fouling (hot films), too large (sonic anemometers) or too slow (propvanes). Neither could noncommercial instruments, such as the thrust anemometer (Smith, 1980a), the fluidic anemometer (Neradka, 1973) or the anemoclinometer (Wesely *et al.*, 1972), be easily adapted for our purposes, and certainly not at the time the development of the new instrument was started. Another instrument for wind measurements in the wave zone, a special type of hot wire (Wills, 1976), was not fit for use during longer periods at sea. These considerations led to the development of the new instrument, the results of which are presented in this paper.

2. Basic design

The instrument has been called a pressure anemometer (PA) and it is in principle a combination of six pressure tubes, arranged in three sets of two. The tubes in each set point in opposite directions, so if one tube points upwind, the other is directed downwind. In the windward tube, the wind causes an overpressure; in the leeward tube, an underpressure. The pressure difference, indicated by a differential pressure transducer, is a measure for the wind component along the tubes. The three sets are mutually orthogonal, so from the ratios of the signals of the transducers we can derive the wind direction and after that, from the direction and one of the signals, the wind speed.

An important feature of the instrument is a flow of clean air, which is forced through the tubes. This flow, from a compressor or a gas bottle, is intended to keep spray and waves outside the instrument.

Figure 1 shows the basic setup for one set or, as we shall indicate it now, for one component. The pressure difference between the windward and leeward arm is measured at the pressure ports, indicated by 3 in Fig. 1. Clean, pressurized air is forced through the vertical leg of the component, enters the pressure tubes through the constrictions (2), and flows out to the atmosphere. The constrictions are needed to prevent the wind from blowing freely through the instrument.

As an alternative to the pressure measurement, one could also measure the velocity difference in the arms, using hot wires. This, however, requires relatively wide constrictions and a low overpressure of the pressurized air, thus jeopardizing the protection of the instrument (Oost 1981). Therefore, only the pressure sensing type has been developed further.

3. Directional sensitivity

The wind direction must be calculated from the ratios of the signals of the three components. Therefore, these ratios must be monotonic functions of the angle between the wind direction and the component axes over a full quadrant. With the elementary arrangement

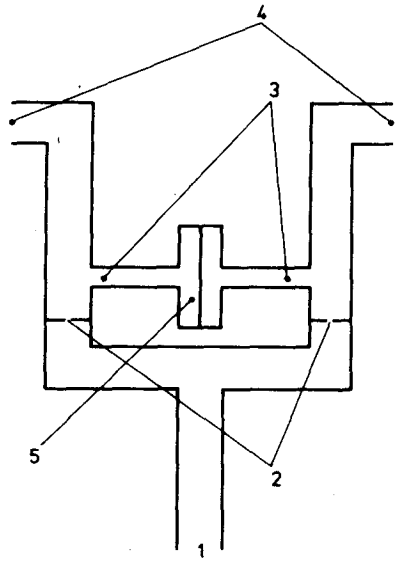

FIG. 1. Principle of the anemometer: (1) inflow tube and support; (2) constrictions; (3) pressure ports; (4) outflow and sensing ports; (5) pressure sensor..

of Fig. 1, this is not the case. The problems lie, as might be surmised, at the leeside; the wake there causes an underpressure which is stronger when the component is at a small angle to the wind, than when it is aligned with it. The pressure at the windward side changes in an approximately cosine fashion with the wind direction, so for small angles the change in pressure there is very slight. Thus the resulting change in pressure difference is mainly determined by the pressure change at the leeside. This behavior is depicted in Fig. 2, together with a cosine function, which may be considered as the ideal relation (Smith, 1980a).

As a consequence, the interpretation of data becomes ambiguous, so we must find a configuration with a better direction response. We obtained it, after a number of attempts, by distributing the outflow and sensing ports along a hollow ring. In this configuration each outlet port in Fig. 1 has been replaced by a hollow ring. The axis of the ring is parallel to the direction of the original outlet port, so the plane of the ring is perpendicular to the plane of the figure. Each ring has a single opening along its rim where it is connected to the rest of the instrument. On one side of each ring, facing outward, are a number of ports, usually four, which together correspond to the single outlet ports of Fig. 1. Instead of two separate rings, however, we use a single ring with a partition in its central plane (Fig. 3). This single ring is actually a combination of the two separate rings, merged back-to-back.

The reason for the satisfactory angular dependence of this configuration is probably that the airflow along the instrument has to bend around the ring and therefore meets the outflowing air at the leeside at an angle which is different from zero.

We are not aware of any attempt to model the interaction between a jet and an airstream that meets

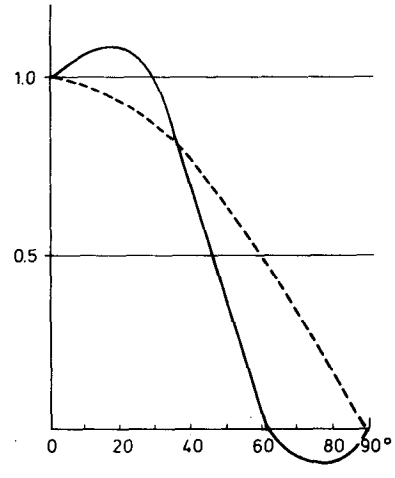

FIG. 2. Relative directional sensitivity of a component (solid line); cosine function (dashed line).

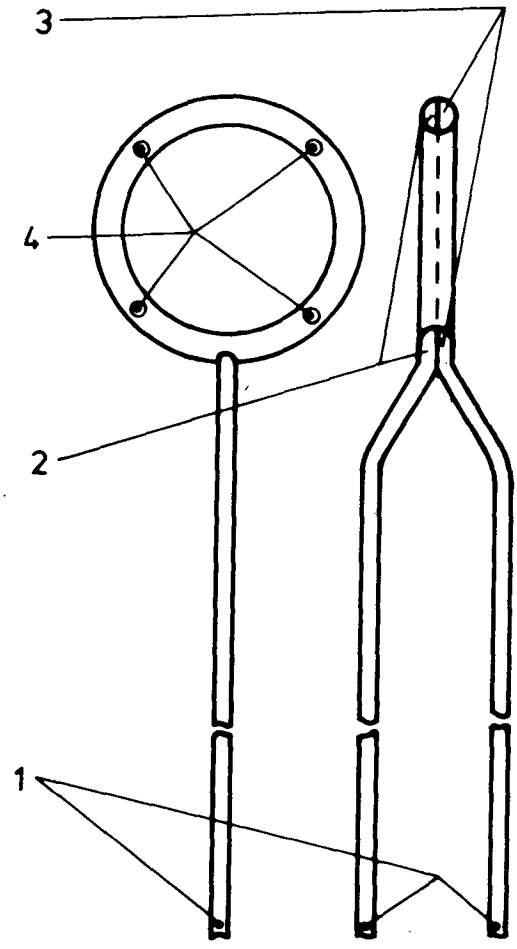

FIG. 3. Ring sensor: (1) flow inlet; (2) left chamber; (3) right chamber; (4) sensor openings.

the jet at an arbitrary angle; moreover, the development of such a model was beyond the scope of this project. This precluded a mathematical analysis of the properties of the sensor rings. We therefore did it empirically.

4. Dimensions of the sensor head

Factors important for the performance of the sensor head are, for example, the dimensions of the ring, the number of openings, size of the openings, the mutual distance of the rings and the orientation of the sensor head.

For constructional reasons we were more or less restricted to a ring diameter of 30 mm and a ring thickness of 5 mm. These length scales are not unfavorable, however, as the frequencies of the corresponding lee eddies are already over 100 Hz at 4 m s^{-1}, which is outside the range we wish to cover (0–40 Hz). Thus the noise, due to these eddies, can be removed with the already needed anti-aliasing filters.

For the number of outlet ports, two considerations are relevant: 1) the signal is a smoother function of the wind direction if the number of ports is higher and 2) the risk of flooding and fouling increases with the number of ports. The first argument is a matter of experience. The second is the consequence of the requirement that the rings must be slender (to avoid excessive mutual interference), so that their internal diameter is not very large compared to the size of the outflow ports. The result is that, starting from the inlet opening, the protective overpressure diminishes at subsequent outlets, and thus the risk that ports are flooded, when the sensor head is hit by a wave, increases with the number of ports. In our experience four ports gave a usable compromise between a smooth direction dependence and good protection. Therefore we adopted this as our standard number.

For the size of the openings the analysis was somewhat more complex. Small openings are favorable for 1) an equal flow rate through all ports (Pascal's law) and 2) a high outflow velocity at a given inlet pressure resulting in a good protection against fouling. Large openings, on the other hand, are desirable for 1) little turbulence in the outflowing air, resulting in a low noise level as far as this is due to the internal flow, 2) a low minimum of the useful velocity range and 3) high sensitivity (= signal level at a given windspeed). In view of conflicting requirements, i.e., a high outflow velocity at a given inlet pressure, and a low minimum of the useful velocity range, a series of experiments was performed in which the direction sensitivity was measured as a function of various parameters. The port diameters in these experiments ranged from 0.4 to 1.0 mm. The rings used were of our standard size with four ports.

Fig. 4 shows two examples from this series. In Fig. 4a the size of the ports is 0.6 mm, in Fig. 4b, 0.8 mm;

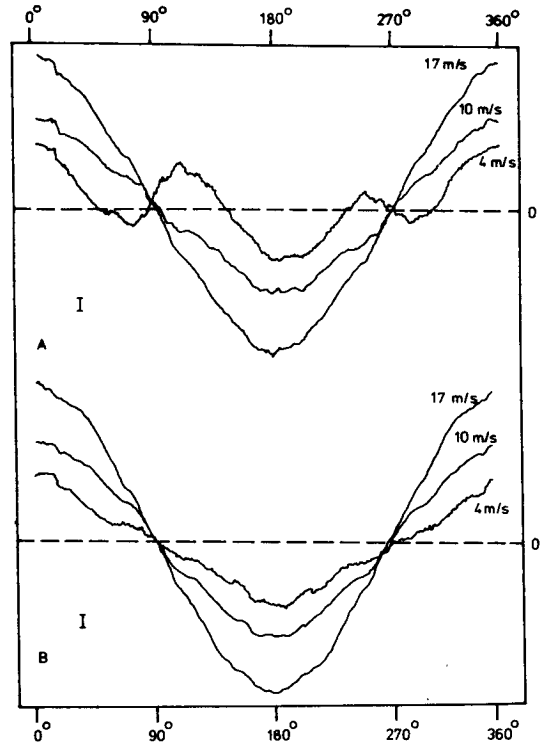

FIG. 4. Signal as function of the angle between the wind direction and the axis of a ring sensor. Ring diameter 30 mm; ring thickness 5 mm. Inlet pressure (in both cases): 0.2 bar. The vertical bar indicates 0.05 V at 4 m s^{-1}, 0.25 V at 10 m s^{-1} and 0.5 V at 17 m s^{-1}. The diameter of the sensor openings was 0.6 mm in case A and 0.8 mm in case B. The horizontal scale in cases A and B is slightly different.

in both instances the inlet pressure of the PA was 0.2 bar. Note the difference in behavior of the curves for 4 m s^{-1} in Figs. 4a,b. With the smaller openings the angular dependence shows the same unsatisfactory behavior as in Fig. 3 for the region 60 to 90 deg and the corresponding regions in other quadrants. (We neglect a small offset at 90 deg, due to a less than perfect match of the internal flows.) The conclusion from Fig. 4a is that in this case the useful velocity range has its lower limit somewhere between 4 and 10 m s^{-1}, which would be a serious restriction. With the larger openings of Fig. 4b the direction dependence is well behaving at 4 m s^{-1}. This is mainly due to the change in average velocity of the jets at the outflow ports, which is 12 m s^{-1} in case A and 7 m s^{-1} in case B. It appears that this velocity should be less than double the desired minimum of the velocity range. We have not investigated this in detail, mainly because effects due to changes in the Reynolds number, related to the overall dimensions of the ring, also start showing up in this velocity range. It is quite improbable, however, that the minimum velocity could be made much lower than 4 m s^{-1} unless the dimensions of the rings are changed. This was borne out by an experiment in which no internal flow was used and in which the same type

of direction dependence was found as in Fig. 4a, although the useless part was restricted to a somewhat smaller angular range. No further improvement was obtained for port diameters larger than 0.8 mm, so we adopted this value as our standard, together with an inlet pressure of 0.2 bar.

The mutual distance of the rings is another empirically obtained compromise between two conflicting considerations: first, the rings should be as close together as possible to improve on the spatial resolution; second, they should be far apart to prevent excessive mutual interference which would make a useful calibration impossible. It turned out that 150 mm was an acceptable distance.

The complete sensor head consists of three mutually orthogonal rings. We have mounted them in a somewhat unorthodox fashion; i.e., with the instrument upright their centers are on a horizontal circle with a 120° spacing. Their axes have an angle of $\cos^{-1}(2/3)^{1/2}$ to the plane of the centers [$\cos^{-1}(2/3)^{1/2} = 35.26°$]. In this way the axes are mutually orthogonal while we do not need a special very sensitive component for the vertical wind. This is an important advantage because the pressure difference due to the vertical wind would be in the 10 to 50 Pa (0.1 to 0.5 mb) range. Pressure sensors for this range are expensive, difficult to handle and very sensitive to accelerations. For our configuration we need only transducers with a ±500 Pa (±5 mb) range, which are preferable in every respect.

Two main subconfigurations of the rings are possible: 1) the axes of the rings intersect in one point on the central axis of the instrument and 2) the axis of each ring lies in the plane of another ring. The advantage of the first subconfiguration is that the distance between rings is at a minimum, all other dimensions being equal; the advantage of the second is minimum interference. We used the first one.

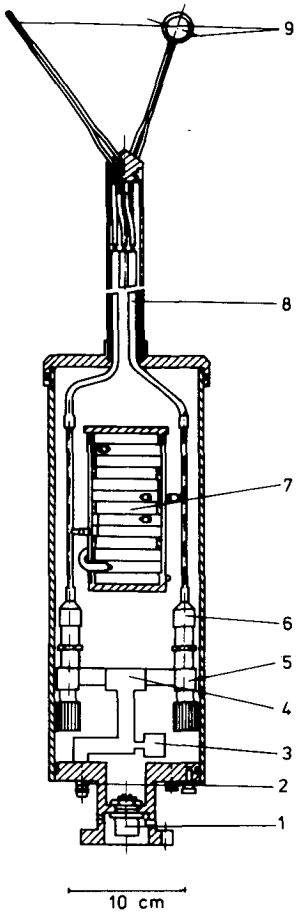

FIG. 5. The pressure anemometer: (1) electric connection; (2) pressure inlet; (3) sensor inlet pressure; (4) manifold; (5) needle valve; (6) laminarizer; (7) differential pressure transducers; (8) stem (approximate length 25 cm); (9) sensor rings. Only two needle valves and laminarizers (of the total of six of each) and two of the three rings have been indicated.

5. The full instrument

The PA has been depicted schematically in Fig. 5. Following the air stream, starting at the inlet (2), we first meet a pressure sensor (3) for the inlet pressure. After the manifold (4), where the airstream is distributed over 6 channels (one for each arm of each component) we come to the needle valves (5) which replace the constrictions of Fig. 1. The airstream then passes a set of laminarizers (6), which have been introduced to suppress turbulent noise at the connections to the pressure transducers (7) that follow the laminarizers. From these connections the air flows through the stem (8) to the sensor rings (9) and out to the atmosphere.

There are 4 pressure transducers at (7). Three of them detect the signals of the various components, whereas the pressure ports of the fourth one (which is identical to the other three) have been shortcircuited. This transducer acts as an acceleration detector; its signal is added to those of the other three with a 180° phase shift. In this way we have diminished strongly the inherent acceleration sensitivity of the instrument.

We use Validyne MP45 pressure transducers, with a natural frequency of 600 Hz. The volume of the pressure cavity is 0.16 cm^3; the transducers can stand a 1 bar overload, making them well-suited for our purpose. The main disadvantage is that they are bulky and heavy compared to more recent instrumentation.

In order to evaluate the frequency response of a single component, we mounted a sensor ring and a hot wire sensor side by side in a wind tunnel and a chopper wheel just downstream of them. When we start rotating the chopper wheel, while the wind is blowing, we introduce wind speed fluctuations, which are the same for both anemometers. The hot wire instrument reacts so fast to wind speed fluctuations that we may consider its response as instantaneous for the frequency range 0–40 Hz. With this supposition, the frequency response of the PA can be derived from the

relative values of the signals of the two instruments at various chopper frequencies and wind speeds. From the results, given in Fig. 6, we draw the inference that the PA, so far as the separate components are concerned, can be used for frequencies of 30–35 Hz (3 dB point).

However, the useful frequency response of the PA is also determined by the mutual distance of the rings. This subject has been treated in a separate article (Oost and Komen, 1983). Some characteristic results from calculations in that article are that wavelengths of 12.5 cm (which correspond to a frequency of 40 Hz at 5 m s^{-1}) are 3 dB lower; for less than 5% loss in amplitude, the wavelength should be larger than 2.5 m and for less than 10% loss it should be larger than 1.5 m.

6. Calibration and data transformation

The signals are not sufficiently smooth functions of the wind direction to approximate them satisfactorily by simple mathematical functions. This is caused both by irregularities of the type apparent in Fig. 4 and by the mutual interference of the rings. We, therefore, had to use a rather extensive calibration and data transformation procedure.

The calibration consists of two parts, i.e., the velocity calibration and the direction calibration.

During the velocity calibration the sensor ring of one of the components (indicated as component 1) is facing the airstream in a wind tunnel. The tunnel is run at a number of wind speeds and the signal of component 1 is recorded. In this way we get a wind speed calibration, valid for one component in one position. Fig. 7 is an example of such a calibration. A regression calculation resulted in the relation

$$u = 0.658 s^{0.479} \qquad (1)$$

in which u indicates the velocity in m s^{-1} and s the signal in mV. One would expect a value of 0.5 for the exponent of s, because the instrument actually measures the wind pressure. As an indicator for the accuracy of the calibration, the standard deviation of the wind speed in each calibration point can be used. It has a value of about 0.6%, except for wind speeds below 4 or over 20 m s^{-1}, where it is in the range of 1 to 2%. There may be a relation between the increase of the standard deviation at high wind speeds and the deviation from the straight line of Fig. 7 in the same velocity range, but we have not gone further into this matter.

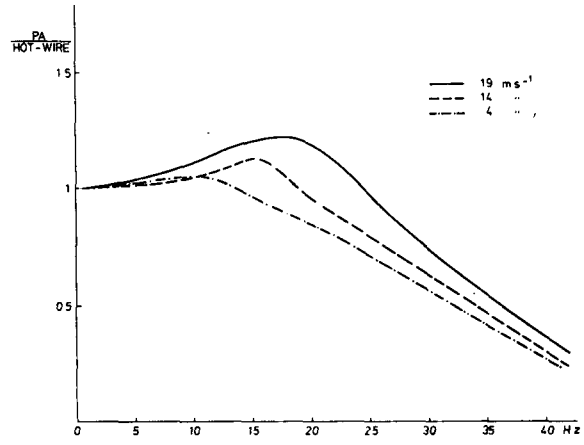

FIG. 6. Ratio of the signals of the pressure anemometer and a hot wire anemometer. The ratio has been normalized to 1 at 0 Hz.

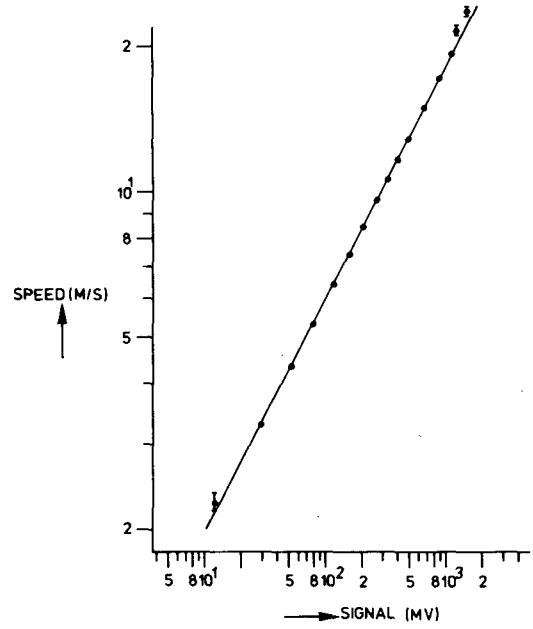

FIG. 7. Velocity calibration of the pressure anemometer. The solid line is the power law relation (1). (See text.)

For the direction calibration the wind tunnel is run at a constant speed and the PA is rotated, both around its body axis (azimuth rotation) and around a horizontal axis perpendicular to the body axis (elevation rotation). To this end the PA is mounted on a calibration platform (Fig. 8), connected to a steering unit. The steering unit automatically scans both the desired azimuth and elevation ranges in steps of 5°.

After the direction calibration, we know in every grid point the values of the signals of the three components and the orientation of the instrument with respect to the wind. The first step in transformation of these figures into quantities which can be used for the interpretation of data, is to assume a cosine direction sensitivity. With this supposition we calculate an apparent wind direction (azimuth and elevation) from the ratios of the signals of the three components. Next we calculate a third factor, again for every grid point, which we call the velocity index. We need it to calculate the wind speed. The concept may be explained as follows. At a certain moment during the

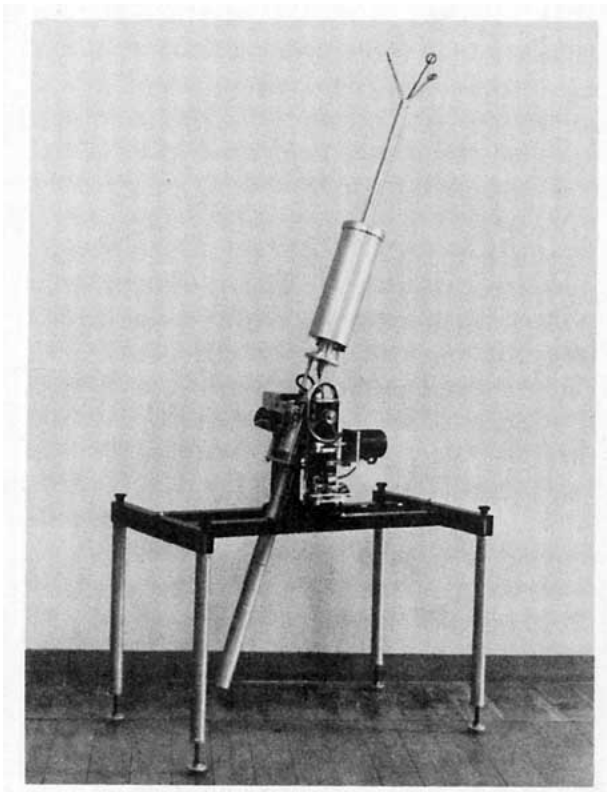

FIG. 8. The calibration platform with the pressure anemometer mounted.

direction calibration, the anemometer finds itself back in the position it occupied during the velocity calibration. In this position one can calculate the wind speed, from the signal of component 1 and the velocity calibration. Therefore, we take the value of the signal of component 1 in this position as a reference. The velocity index for an arbitrary position is then the absolute value of the ratio of the strongest signal (positive or negative) in that position and the reference value just defined.

To illustrate this concept somewhat further, we will describe the use of the velocity index in the interpretation of data. In that case we first calculate, using the strongest signal and the velocity index, the value of the signal which component 1 would have had, if that component had experienced the same windspeed while facing into the wind, i.e., in the position of the velocity calibration. From this value and the velocity calibration, we then determine the wind speed.

To return to the treatment of the calibration data: After we have calculated the apparent azimuth, apparent elevation and velocity index for every grid point, we make a table giving these quantities as functions of the true azimuth and true elevation. When interpreting measured data, however, we wish to know the true angles, but we can only derive the apparent ones from the data. Therefore our table must be inverted in order to give the true azimuth and elevation and the velocity index as functions of the apparent angles. We do this by linear interpolation.

There is still a complication left, namely, that the direction calibration is velocity dependent. To resolve this problem we perform this calibration at a number of windspeeds (usually 3). The interpretation of measured data, however, is now greatly complicated: we know the calibration quantities, derived from the (three) direction calibrations only as functions of the windspeed—which we do not know when we start interpreting data. This forces us to use an iteration procedure containing the following steps:

1) We calculate the values of the apparent azimuth and elevation (which is a straightforward procedure) and a first approximation to the velocity. The last quantity is obtained by taking the square root of the sum of the squares of the three signals and using this value for s in (1). The quantity calculated in this way would be the true wind speed if the direction dependence was a cosine function.

2) Next we use this approximate velocity and the calibration tables to find a value for the velocity index. To this end, we take the values of the velocity index at the appropriate apparent azimuth and elevation from each table and calculate the velocity index for our approximate velocity by interpolation between these values.

3) Step 2 is repeated until we obtain convergence. It usually takes one or two iterations to approximate the end value to within 1 cm s^{-1}.

4) Finally, we calculate the true azimuth and elevation, using the apparent angles and the now known windspeed.

For the calculations, we have to interpolate repeatedly between corresponding values in the three tables. To prevent unnecessary computations, we have calculated the coefficients for these interpolations once and for all for all grid points. Our computer program for the transformation of signal values into physical quantities only uses tables of these coefficients. With our Burroughs B6800 we need less than 3 μs CPU-time per transformation in this way.

This system for the transformation of measured data into values of wind speed, azimuth and elevation has a very wide applicability. It can be used for any anemometer or combination of anemometers for which the ratios of the signals are monotonic functions of the direction. Two main advantages are the capability to handle fairly whimsical direction dependences and the correction of the effect of inaccuracies in the mechanical construction of the anemometer on the results of measurements.

The instrument kept its calibration reasonably well during the field tests. A few runs were analyzed with both the calibration before and after the experiment; the results had mean differences of 3% in windspeed, 2.7° in azimuth and 0.6° in elevation.

7. Field tests

We used the instrument in a number of field tests. The first, with the instrument in its present configuration, was done in the fall of 1980. The experiment consisted of two parts: a technical test, which was performed at the field site of our Institute at Cabauw and an intercomparison with a sonic anemometer at Meetpost Noordwijk, an offshore platform, approximately 9 km off the Netherlands coast and belonging to Rijkswaterstaat (the Netherlands Department of Public Works).

The sonic anemometer in the intercomparison was a Kayo Denki DAT-300, a three dimensional type, with a nonorthogonal sensor array of the familiar type (e.g., see Fox, 1968). Unique to the DAT series is the use of a single set of transducers for each component (Hanafusa *et al.*, 1982). This is possible because each transducer is used alternately as receiver and transmitter. This arrangement has a number of advantages, but the sampling frequency is limited now to 10 Hz, instead of the 20 Hz of earlier types; consequently, we only have spectral information up to 5 Hz.

The sonic had been calibrated in the same way as the PA, though over a smaller azimuth range, in view of the different sensor configuration; the data transformation was conducted in the same way as with the PA. Thus we eliminated imperfections in the construction of the sensor head and deviations from the supposed cosine direction response of the sensors. Some sonic runs were analyzed as well in the conventional way; these analyses gave slight, but significant differences from those for which the full calibration was used. The results presented here are all of the latter type.

We registered our data digitally on magnetic tape. Our data registration system is a Kayser K1280 PCM-system; it has a word length of 12 bits and we used it at a bitrate of 13.5 kHz, resulting in a sampling frequency of about 70 Hz per channel, both for the PA and the sonic. In order to prevent aliasing we used a four pole low-pass Butterworth filter with the PA, with a 3 dB point at 20 Hz. With the sonic we used a much simpler filter, with a 3 dB point at 7 Hz. This difference in the filters caused no problems, thanks to the low energy content of the spectrum beyond 5 Hz.

At Meetpost Noordwijk the PA and the sonic were mounted below each other at the end of a 10 m boom, one instrument upright, the other one inverted. During most of the runs the PA was upright, the sonic inverted.

The boom was at the south side of the platform, 6.3 m, above the mean water level. The sensors of the PA were 1.27 m above (or below) the boom; the center of the sensor of the sonic was 0.62 m below (or above) it.

During a period of two weeks we made 27 runs of 30 min duration each; 8 of these were not suitable for analysis (mainly technical tests). The mean values for windspeed, azimuth and elevation of the remaining 19 runs are presented in Table 1; the windspeed of the sonic has been reduced to the level of the PA sensors in this table, with the use of a ln-profile and a roughness length of 0.3 mm.

The agreement between the windspeeds is satisfactory; the correlation coefficient is 0.992. The windspeeds of the sonic are, however, systematically some-

TABLE 1. Mean values for windspeed, azimuth and elevation. Azimuth directions are given clockwise from north. The second column lists position of the pressure anemometer (PA): (up) above the boom and (down) below it. The sonic sensor always occupies the opposite position. The speed of the sonic has been reduced to the level of the PA.

		PA			Sonic		
Run	Position PA	Speed ($m\ s^{-1}$)	Azimuth (deg)	Elevation (deg)	Speed ($m\ s^{-1}$)	Azimuth (deg)	Elevation (deg)
1	up	6.8	209.1	2.8	6.8	216.4	−5.2
2	up	5.9	195.6	1.6	6.1	195.7	−6.0
3	up	6.3	193.8	1.1	6.7	195.9	−6.2
4	up	7.0	202.5	1.5	7.3	204.3	−6.0
5	up	7.0	202.9	1.9	7.4	206.6	−5.4
6	up	8.9	210.9	2.2	9.1	213.4	−5.3
7	up	8.7	194.9	2.1	8.9	197.9	−5.5
9	up	11.3	267.1	3.1	11.6	267.5	−3.5
10	up	13.3	258.6	4.0	13.6	254.9	−3.7
11	up	13.9	256.0	3.2	14.1	251.9	−3.4
12	up	12.9	250.6	4.0	13.2	247.4	−3.5
13	up	10.8	266.4	4.4	11.2	263.3	−2.9
15	up	12.0	238.7	2.8	12.2	238.2	−4.5
19	up	7.9	232.7	3.3	8.2	228.7	−4.8
20	down	10.5	228.9	−4.1	10.8	223.8	3.0
21	down	11.5	239.3	−3.3	11.9	235.9	3.2
22	down	11.0	239.7	−3.5	11.4	235.3	3.2
23	up	11.9	244.2	3.5	12.2	250.2	−3.9
24	up	15.0	281.1	5.3	15.5	273.1	−3.0

what higher than those of the PA. We attribute this mainly to imperfections in the calibration such as 1) the sonic was calibrated without its rotor, 2) during the calibration the sonic was at a different spot in the wind tunnel than the PA, and 3) the instruments have different fill factors in the wind tunnel. The difference between the azimuth values of the sonic and the PA is 0°.7 ± 4°. The rather large spread is caused by a systematic shift of the difference with the azimuth; at azimuth values around 200° the azimuth, registered by the PA is lower than that of the sonic, whereas in the neighborhood of 250° we have the reverse situation. This leads us to the conclusion that the windfield was distorted and that the low mean value must be considered accidental.

The elevation values show the distortion still more clearly; they also give a strong indication that it is due to our boom and not to the anemometers themselves or the platform because the elevation is always positive if an instrument is above the boom and negative when below it—independent of the type of anemometer.

The consistent picture which emerges from these experiments indicates that the performance of both instruments is comparable as far as it concerns mean values, although the distortion precludes a detailed comparison of the results. In the future, we expect to give a more detailed and quantitative analysis of the distortions, as well as a comparison with models for them like those of Wyngaard (1981) and Dyer (1981).

In Fig. 9 we show spectra from both instruments,

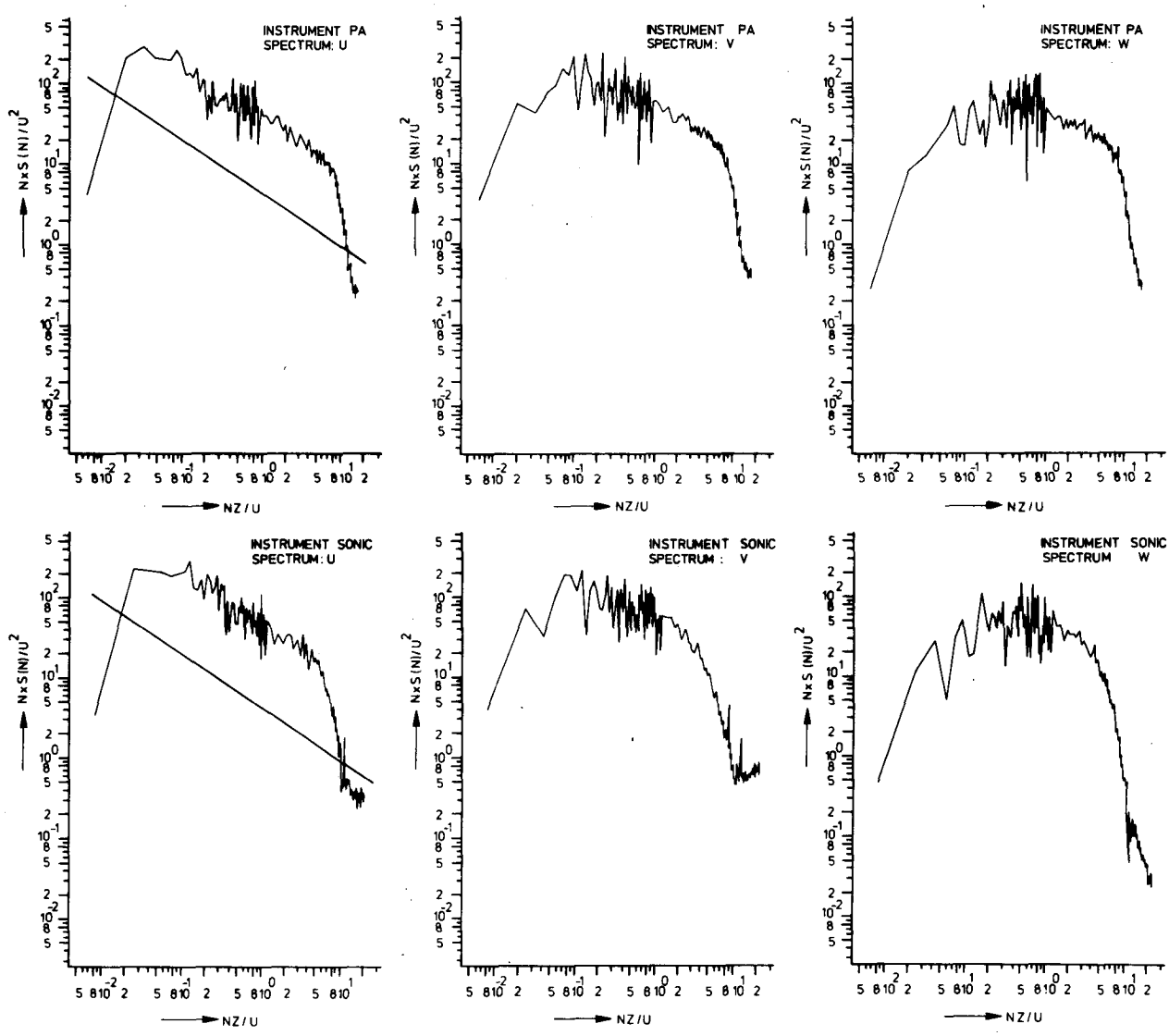

FIG. 9. Nondimensional spectra. The spectra in the upper row are from the pressure anemometer; those of the lower row from the sonic. The spectra in the first column are *u*-spectra, those in the second *v*-spectra and those in the third one *w*-spectra. The straight line in both *u*-spectra has a $-\frac{2}{3}$ slope which is characteristic for an inertial subrange. Low- and high-frequency spectra were calculated separately. No smoothing filters were used.

calculated with a standard FFT procedure. The high and low frequency parts were calculated separately. For the low frequency part, we selected every tenth sample of the 30 min run; these were filtered with a numeric low-pass Butterworth filter before transformation. For the high frequency part, we only used the first three minutes of a run, without any further treatment. We did not apply any smoothing filters.

All spectra show a $-\frac{2}{3}$ slope, characteristic of an inertial subrange. In all cases this slope ends at the high frequency side in the cutoff of the filters. No indications of disturbing influences are manifest in the spectra.

As a final check we calculated C_{10}, the drag coefficient at 10 m height for all runs of Table 1. For this, we proceeded as follows:

From the mean values for the vertical turbulent momentum flux $\overline{u'w'}$ and the mean velocity U we derived values for the drag coefficient C_Z at the height of the sensor concerned. We did this for all runs and for both instruments. To reduce these values to 10 m height we then derived, with the help of a rough estimate of the humidity, values for the temperature T and the vertical heat flux $\overline{w'T'}$ from the sonic anemometer [our method is slightly different from the one given in Schotanus *et al.* (1983); we use an estimate of the relative humidity instead of the Bowen ratio]. With the values now available of $\overline{u'w'}$, $\overline{w'T'}$ and T, and the supposition that air near the water surface is saturated with moisture, we calculated approximate values for the Monin–Obukov length L. For these calculations we needed the transfer coefficients C_T for heat and C_E for moisture; we used the values given in Large and Pond (1982), viz. $10^3C_T = 0.75$ in a stable and $10^3C_T = 1.13$ in an unstable situation and $10^3C_E = 1.15$. Finally the C_Z-values and the mean windspeed can be reduced to 10 m, height, with the use of the profile formulas given, e.g., by Large and Pond and the z/L values just derived.

The results are shown in Table 2. The agreement between the C_{10}-values of both instruments is exceptionally good, apart from those of run 24. In that case, however, the wind at the level of the PA was blowing slightly from the direction of the platform, making this value unreliable. We consider the agreement of the remaining runs as another example of the comparable quality of the two instruments. Although the C_{10} values (except those of run 19) are in general agreement with those in the literature (e.g., Garratt, 1977; Wu, 1980; Smith, 1980b; Large and Pond, 1981), it must be kept in mind that the wind field is distorted, probably due to the boom, so this correspondence may change if more corrections are applied. These corrections are deferred to a later publication; the main purpose of the present report is to give a description of the new anemometer and calibration system and to show that the results of PA and sonic are in agreement when the instruments are used under the same circumstances.

TABLE 2. Drag coefficients. All wind speeds have been reduced to 10 m height; C_{10} is the drag coefficient at 10 m height. Values given are means and standard deviations of ten 3 min values. Notation as in Table 1.

		PA		Sonic	
Run	Position PA	Speed (m s^{-1})	C_{10} (×1000)	Speed (m s^{-1})	C_{10} (×1000)
1	up	6.7 ± 0.1	1.1 ± 0.5	6.9 ± 0.2	1.0 ± 0.3
2	up	6.0 ± 0.2	1.0 ± 0.3	6.2 ± 0.2	0.9 ± 0.3
3	up	6.4 ± 0.2	1.2 ± 0.6	6.7 ± 0.2	1.1 ± 0.5
4	up	7.1 ± 0.2	1.1 ± 0.5	7.4 ± 0.2	0.9 ± 0.3
5	up	7.3 ± 0.3	0.7 ± 0.4	7.7 ± 0.3	0.6 ± 0.4
6	up	9.1 ± 0.5	1.5 ± 0.3	9.3 ± 0.5	1.2 ± 0.2
7	up	8.9 ± 0.4	1.8 ± 0.4	9.1 ± 0.4	1.5 ± 0.5
9	up	11.5 ± 0.4	1.5 ± 0.5	11.8 ± 0.4	1.2 ± 0.3
10	up	13.8 ± 0.4	1.5 ± 0.5	13.9 ± 0.4	1.2 ± 0.2
11	up	14.4 ± 0.8	1.2 ± 0.3	14.6 ± 0.8	1.3 ± 0.3
12	up	13.4 ± 1.0	1.5 ± 0.4	13.6 ± 1.0	1.5 ± 0.2
13	up	11.1 ± 0.6	1.6 ± 0.4	11.5 ± 0.5	1.4 ± 0.3
15	up	12.3 ± 0.5	1.3 ± 0.3	12.5 ± 0.6	1.3 ± 0.3
19	up	8.2 ± 0.6	0.7 ± 0.1	8.6 ± 0.7	0.8 ± 0.1
20	down	11.4 ± 0.5	1.2 ± 0.5	11.7 ± 0.5	1.3 ± 0.5
21	down	12.3 ± 0.3	1.5 ± 0.3	12.7 ± 0.3	1.5 ± 0.4
22	down	11.7 ± 0.2	1.3 ± 0.2	12.1 ± 0.2	1.2 ± 0.3
23	up	12.3 ± 0.9	1.1 ± 0.3	12.5 ± 0.8	1.0 ± 0.2
24	up	15.7 ± 0.8	2.9 ± 0.6	16.0 ± 0.8	1.5 ± 0.3

8. Final remarks

The PA is now at a stage where it can be used with confidence, provided one takes sufficient care with respect to the calibration and the interpretation of the data. This makes application for routine purposes rather impractical; one should realize that it has been developed as a research instrument. A special application that deserves mentioning is the use in arctic conditions: the PA contains no moving parts and the pressurized air can be heated to de-ice the instrument.

Since the measurements, reported on here, have been completed, more series were taken, in which the PA was brought closer to the water surface. During those measurements its sensor system was submerged a few times, when hit by a wave. To our disappointment the air pressure did not keep the instrument dry inside, contrary to our experiences during laboratory tests. It showed that the construction of the sensor rings is rather critical. The problem can be alleviated by giving the item the shape of an inverted "J." If the instrument is used close to the water, it is upside down compared to Fig. 5, so with the J-stem, the sensor head is upright again. This has the advantage that the lowest openings, which are most exposed, are those with the highest overpressure (compare Section 4). The disadvantage of this shape, that an azimuth sector is excluded, is of no consequence because the direction of the platform or mast to which the instrument has been fixed can be used for that purpose. This change hardly affects other properties of the instrument.

Acknowledgments. The author gratefully acknowledges the help of all the people who have contributed to the development of the pressure anemometer. Special mention is given to: Mr. J. W. Schaap for his many contributions in all stages of the project; Mr. E. H. W. Worrell for his design and construction of the electronics; Mr. L. P. H. van der Woerd for his design of the instrument body, the KNMI-machine shop, for the perfection with which they built the instrument and Mr. C. Kraan, M.Sc. for his support in the later part of the project and especially for his painstaking labors in the disentanglement of the data.

REFERENCES

Chalikov, D. V., 1978: The numerical simulation of wind-wave interaction. *J. Fluid Mech.*, **87,** 561–582.

Dyer, A. J., 1981: Flow distortion by supporting structures. *Bound.-Layer Meteor.*, **20,** 243–251.

Fox, L. H., 1968: Continuous wave three-component sonic anemometer. Final Report, AFCRL-68-0180, Bolt, Beranek and Newman Inc., 57 pp.

Garratt, J. R., 1977: Review of drag coefficients over oceans and continents. *Mon. Wea. Rev.*, **105,** 915–929.

Gent, P. R., 1977: A numerical model of the air flow above water waves, Part 2. *J. Fluid Mech.*, **82,** 349–369.

——, and P. A. Taylor, 1976: A numerical model of the air flow above water waves. *J. Fluid Mech.*, **77,** 105–128.

Hanafusa, T., T. Fujitani, Y. Kobori and Y. Mitsuta, 1982: A new type sonic anemometer-thermometer for field operation. *Pap. Meteor. Geophys.*, **33,** 1–19.

Janssen, P. A. E. M., 1982: Quasilinear approximation for the spectrum of wind-generated waves. *J. Fluid Mech.*, **117,** 493–506.

Large, W. G., and S. Pond, 1981: Open ocean flux measurements in moderate to strong winds. *J. Phys. Oceanogr.*, **11,** 324–336.

——, and ——, 1982: Sensible and latent heat flux measurements over the ocean. *J. Phys. Oceanogr.*, **12,** 464–482.

Melville, W. K., 1977: Wind stress and roughness length over breaking waves. *J. Phys. Oceanogr.*, **7,** 702–710.

Miles, J. W., 1957: On the generation of surface waves by shear flows. *J. Fluid Mech.*, **3,** 185–204.

——, 1959: On the generation of surface waves by shear flows, Part 2. *J. Fluid Mech.*, **6,** 568–582.

Neradka, V. F., 1973: Development of a meteorological two-axis wind sensor. Final Report, Office of Naval Research, 51 pp. [AD 755740]

Oost, W. A., 1981: The pressure anemometer—a new kind of wind vector measuring device. *WMO Ser. on Instruments and Observing Methods,* Rep. 9, 25–31.

——, and G. J. Komen, 1983: Spatial resolution of the pressure anemometer. *J. Climate Appl. Meteor.*, **22,** 2085–2094.

Riley, D. S., M. A. Donelan and W. H. Hui, 1982: An extended Miles theory for wave generation by wind. *Bound.-Layer Meteor.*, **22,** 209–225.

Schotanus, P., F. T. M. Nieuwstadt and H. A. R. de Bruin, 1983: The use of a sonic anemometer for measurements of heat and moisture fluxes. *Bound.-Layer Meteor.* (in press).

Smith, S. D., 1980a: Evaluation of the Mark 8 thrust anemometer-thermometer for measurement of boundary layer turbulence. *Bound.-Layer Meteor.*, **19,** 273–292.

——, 1980b: Wind stress and heat flux over the ocean in gale force winds. *J. Phys. Oceanogr.*, **10,** 709–726.

Wesely, M. L., C. B. Tanner and G. W. Thurtell, 1972: An improved pressure sphere anemometer. *Bound.-Layer Meteor.*, **2,** 275–283.

Wills, J. A. B., 1976: A submerging hot wire for flow measurements over waves. *DISA Inf.*, **20,** 31–34.

Wu, J., 1980: Wind-stress coefficients over sea surface near neutral conditions—A revisit. *J. Phys. Oceanogr.*, **10,** 727–740.

Wyngaard, J. C., 1981: The effects of probe-induced flow distortion on atmospheric turbulence measurements. *J. Appl. Meteor.*, **20,** 784–794.